Review of Scientific Instruments ARTICLE pubs.aip.org/aip/rsi

Optical fiber strain sensor with high and tunable sensitivity

Cite as: Rev. Sci. Instrum. 94, 115003 (2023); doi: 10.1063/5.0154895
Submitted: 16 April 2023 • Accepted: 19 October 2023 •
Published Online: 8 November 2023

Shiwei Yang,[1] Qiang Zhang,[1,2,a)] Xiaobo Li,[1] Quansen Wang,[1] and Yongmin Li[1,2,a)]

AFFILIATIONS

[1] State Key Laboratory of Quantum Optics and Quantum Optics Devices, Institute of Opto-Electronics, Shanxi University, Taiyuan 030006, China
[2] Collaborative Innovation Center of Extreme Optics, Shanxi University, Taiyuan 030006, China

[a)] **Authors to whom correspondence should be addressed:** qzhang@sxu.edu.cn and yongmin@sxu.edu.cn

ABSTRACT

We demonstrate a fiber-optic strain sensor with high and tunable sensitivity by constructing a Fabry–Perot interferometer with tunable stretching length. By improving the ratio of stretching length to interference length for the proposed sensor, the measured strain sensitivity is up to 1932 pm/$\mu\varepsilon$, which is an order of magnitude higher than the maximum value of reported fiber-optic strain sensors so far. The sensitivity for a prepared sensor could be also tuned conveniently by changing the stretching length, and experimental results show that the sensitivity could be tuned from 1932 to 978 pm/$\mu\varepsilon$ by reducing the stretching length from 12 to 6 mm. Furthermore, the proposed device is economical, straightforward, robust, and reproducible. The advantages make the proposed device promising in practical applications.

I. INTRODUCTION

Optical fiber strain sensors are of great value in varied exciting applications, such as marine geophysics,[1,2] rechargeable lithium-ion batteries,[3] aircraft health monitoring,[4,5] composite materials,[6] and biomechanics,[7] owing to the promising advantages of miniature size, inertness, biocompatibility, low cost, immunity to electromagnetic interference, and suitability to be embedded into structures. In recent years, various fiber-optic devices are used to measure ambient strain, such as Bragg gratings,[8–11] long-period gratings,[12–14] Mach-Zehnder interferometer,[15–18] and Fabry–Perot interferometer.[19–24] Strain sensors using fiber Bragg grating play an important role in strain measurement because of the advantage of wavelength division multiplexing, but the maximum sensitivity of those strain sensors is less than 10 pm/$\mu\varepsilon$.[8–10] The strain sensors based on long-period gratings could obtain higher sensitivity, and the maximum strain sensitivity reported using S-shaped long-period grating is 29.3 pm/$\mu\varepsilon$.[12] However, the cross sensitivity of temperature for fiber-grating strain sensors needs to be eliminated, and the processing systems of fiber gratings are expensive. Compared with fiber gratings, fiber-optic interferometers based on special optical fibers or fiber-optic microstructures could further improve the sensitivity. For example, the sensitivity of the Mach–Zehnder strain sensor using dissimilar-doping dual-core fiber is up to 102 pm/$\mu\varepsilon$.[18] Another common fiber-optic interferometer for strain measurement is Fabry–Perot interferometer (FPI),[19–24] where the reflective principle is beneficial to simplify the sensor structure. In order to improve the strain sensitivity, several artful sensors are demonstrated, such as reducing the cavity length of FPI,[19] cascading FPIs,[20] in-fiber rectangular air bubble,[21] pillar-in-bubble cavity,[22] and parallel FPIs in multicore fiber,[23] and the maximum strain sensitivity is 56.69 pm/$\mu\varepsilon$ by fabricating a pillar-in-bubble FPI with a CO_2 laser machining system.[22] For the strain sensors based on fiber-optic interferometers, the high sensitivity is owing to the expensive special optical fibers or complex machining systems, such as dissimilar-doping dual-core fiber, photonic crystal fiber, multicore fiber, femtosecond laser, and CO_2 laser. Therefore, new methods need to be developed further for economic high-sensitivity strain sensors.

In this paper, an ultrasensitive fiber-optic strain sensor is demonstrated by constructing an FPI with a large ratio of stretching length to interference length. In our experiments, the measured strain sensitivity for the sensor with 9.3 μm cavity length is up to 1932 pm/$\mu\varepsilon$ that is 19 times larger than the maximum value for all reported fiber-optic strain sensors[18] so far. Meanwhile, the sensitivity could be tuned artificially by changing the position of the fixed points, and experimental results show that the sensitivity of

the device with 9.3 μm cavity length could be tuned from 1932 to 978 pm/$\mu\varepsilon$, which is beneficial to different practical applications. In addition, the cost of the proposed device is very low for the economical processing equipment and raw materials. Therefore, the proposed device shows attractive potentialities for practical applications.

II. FABRICATION AND PRINCIPLE

The schematic diagrams of the proposed sensor and measuring setup are shown in Fig. 1. The constructing method of the sensor is simple and reproducible. First, some raw materials need to be prepared, including two single mode fibers (SMFs, FullBand® Low Water Peak Single-mode Fiber, YOFC) with a mode field diameter of about 9.8–10.8 μm and the effective group refracting index of 1.467 at 1550 nm and a silica capillary (SC, Beijing Xingyuan Aote Technology Co., Ltd.) with an inner diameter of 130 μm and outer diameter of 200 μm. It should be noted that the inner diameter of the SC is important for the sensor because the fringe visibility of the FPI will decrease when the inner diameter of the SC increases, and the SMFs cannot move freely when the inner diameter is less than 130 μm. Second, the coatings of two SMFs are removed by a commercialized optical fiber stripper (FiberHome Telecommunication Technologies Co., Ltd.) and further wiped with alcohol to remove surface residue and stains. The end faces of SMFs are prepared and inspected using a fiber cleaver (S326A, FITEL) and fiber inspection scope (FS201, Thorlabs) to ensure that the end faces are flat, smooth, and vertical. Attention is also paid that the bare SMFs are not in contact with any objects to prevent pollution and damage. The two SMFs are inserted into the SC and the two smooth end faces form an FPI, as shown in Fig. 1. Third, the relative position between the right SMF and the SC is fixed by using an instantaneous adhesive (401, LOCTITE), and the position of the left SMF needs to be optimized according to the reflected spectrum of the FPI from the optical spectrum analyzer (OSA, OSA203C Fourier trans-form Optical Spectrum Analyzer, Thorlabs). After optimizing the relative position between the left SMF and the SC, they need to be fixed with the same type of instantaneous adhesive. Figure 1(b) shows a representative optical picture of the sensor and micrograph of the two SMFs in the silica capillary. In our experiments, a broadband source (BBS, OELSC-100 MIR Supercontinuum Light Sources, O/E Land Inc.) with a wavelength range of 1.4–2 μm and a fiber-optic circulator [FOC, CRI-1550-3-P-900-1-FA Polarization Insensitive Optical Circulator, Advanced Fiber Resources (Zhuhai) Ltd.] are used to couple light into the sensor and the OSA, as shown in Fig. 1. The proposed FPI strain sensor is fixed on two precision single-axis linear stages with differential adjuster (DM12, PT1A, Thorlabs), where the fixed points are P0 and P1. When axial strain is imposed to the sensor by adjusting the distance between the two precision linear stages, the stretching length, which is the length of the SC between the fixed points P0 and P1, will be lengthened, the cavity length of the sensor increases, and the corresponding reflective spectrum of the FPI sensor will shifts. Therefore, the axial strain can be achieved by monitoring the shift of the reflective spectrum of the FPI sensor.

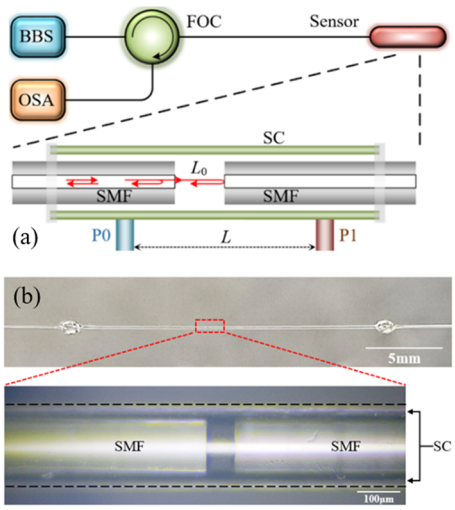

FIG. 1. (a) Schematic diagrams of the proposed strain sensor and measuring setup, including the broadband source (BBS), fiber-optic circulator (FOC), and optical spectrum analyzer (OSA). Two single mode fibers (SMFs) are inserted into silica capillary (SC) to form two-beam FPI. (b) Optical pictures of the sensor.

According to the two-beam interference theory, the normalized reflected intensity I_{ref} from the FPI sensor can be modeled as

$$I_{ref} = R_1 + (1-\alpha_1)^2(1-\alpha_2)(1-\gamma)^2(1-R_1)^2R_2 + 2\sqrt{R_1R_2(1-\alpha_2)}(1-\alpha_1)(1-\gamma)(1-R_1) \times \cos(4\pi n_{air}L_0/\lambda + \pi), \quad (1)$$

$$R_1 = R_2 = (n_{cor} - n_{air})^2/(n_{cor} + n_{air})^2, \quad (2)$$

where R_n is the reflection coefficient of the two SMFs; γ is the transmission loss; L_0 is the FP interference length, which equals the gap between the two SMFs; n_{cor} and n_{air} are the refractive indices of the SMF and air; α_1 and α_2 are the mirror loss; and λ is the optical wavelength in vacuum. According to Eq. (1), the m-order resonant wavelength of the FPI can be calculated by

$$\lambda_m = 2L_0n_{air}/m. \quad (3)$$

When the strain $\varepsilon = \Delta L/L$ is imposed to the sensor, L_0 and λ_m will become $L_0 + \Delta L$ and $\lambda_m + \Delta\lambda_m$. ΔL is the corresponding displacement of the translation stages, and L is the stretching length between the two fixed points on the two precision linear stages. The relationship between $\Delta\lambda_m$ and the strain ε can be expressed as[22]

$$\frac{\Delta\lambda_m}{\varepsilon} = \lambda_m\frac{L}{L_0}. \quad (4)$$

From Eq. (4), the strain sensitivity is proportional to stretching length L and the resonant wavelength λ_m, and is in inverse proportion to the interference length L_0. Therefore, the sensitivity could be improved by increasing the stretching length L and the resonant wavelength λ_m and decreasing the interference length L_0.

Another advantage of the proposed sensor is that the strain sensitivity could be tuned conveniently even though the sensor is completed. From Eq. (4), the strain sensitivity is proportional to the stretching length, so the sensitivity could be tuned by changing the

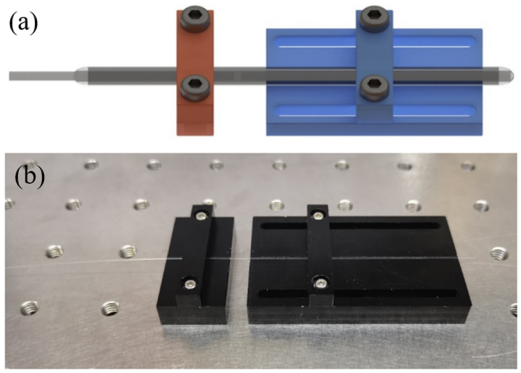

FIG. 2. (a) Schematic diagrams of the strain sensor with tunable stretching length between the fixed points. (b) Optical pictures of the tunable stretching jigs.

stretching length, even though the proposed sensor is completed. Figure 2 shows the schematic diagrams of the strain sensor with tunable stretching length between the fixed points and optical pictures of the tunable stretching jig in the experiments. The left jig is fixed and the right jig is tunable. As shown in Fig. 2, a suitable sensitivity for various practical applications could be obtained by choosing different stretching lengths between the fixed points.

III. EXPERIMENTAL RESULTS AND DISCUSSION

In our experiments, several sensors are constructed to demonstrate the sensing principle. Figure 3(b) shows two representative measured reflected spectra of the sensors. The cavity lengths of the FPI strain sensors are 13.8 and 9.3 μm according to Eq. (3), and the corresponding fringe visibilities are 22 and 16 dB, respectively. To corroborate the experimental results in Fig. 3(b), we calculated the corresponding normalized reflective spectra of the sensors according to Eqs. (1) and (2), as shown in Fig. 3(a), where the calculated parameters are $n_{cor} = 1.46$, $n_{air} = 1$, $\alpha_1 = \alpha_2 = 0.004$, and $\gamma = 0.20$ and 0.05 for the sensors with 13.8 and 9.3 μm cavity lengths, respectively. The measured data are consistent with the calculated results.

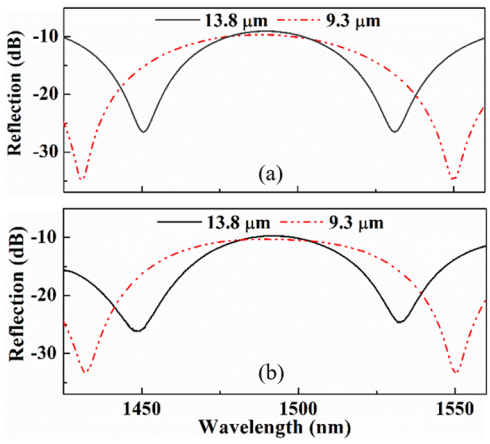

FIG. 3. (a) Calculated and (b) measured reflective spectra of the sensors.

To corroborate the practical application of the proposed sensors, we investigate the response of the sensors to the strain. As shown in Figs. 1 and 2, the FPI strain sensor is fixed between two translation stages, and the stretching length L could be tailored by changing the positions of the two fixed points. When strain is imposed to the proposed FPI sensor, the SC between the fixed points is stretched, and the cavity length L_0 and the m-order resonant wavelength λ_m of the FPI sensor increase. In our experiments, two different stretching lengths L are designed to demonstrate the tunable sensitivity of the proposed strain sensor, where the two different stretching lengths are 12 and 6 mm, respectively. Figure 4 shows the reflective spectra evolution patterns of the sensor with 9.3 μm cavity length as the strain changes from 0 to 25 $\mu\varepsilon$. The dip wavelength λ_m gradually increases as the strain enlarges from 0 to 25 $\mu\varepsilon$. The shift $\Delta\lambda_m$ with a stretching length of 12 mm is two times of that with a stretching length of 6 mm. To evaluate the strain sensitivity, we trace the $\Delta\lambda_m$ of dip wavelength (1550.45 nm) as the strain changes. Figure 4(c) shows that the sensitivities of the sensor with stretching lengths of 6 and 12 mm are 978–1932 pm/$\mu\varepsilon$, respectively. The measured strain sensitivities are close to the calculated sensitivities of 989–1979 pm/$\mu\varepsilon$ according to Eq. (4). The differences between the measured sensitivity and the calculated sensitivity may result from the measured errors of the stretching lengths. Similar measured results have been obtained for other sensors. In our experiments, the measured sensitivity for the strain sensor with 9.3 μm cavity length is up to 1932 pm/$\mu\varepsilon$, which is 19 times larger than the maximum

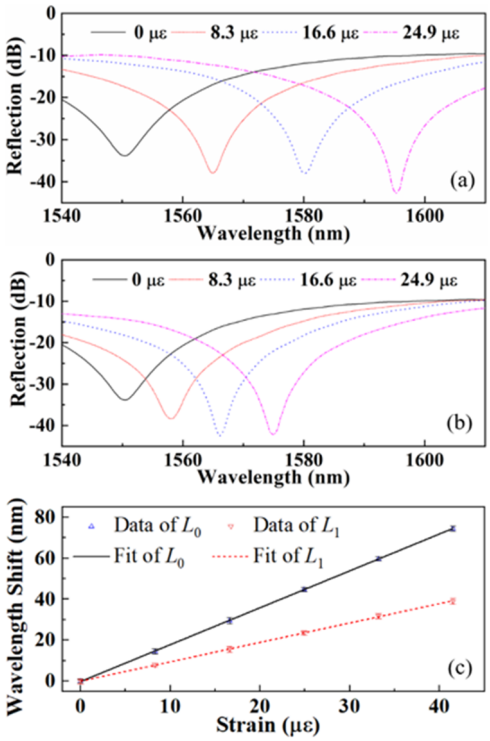

FIG. 4. Reflected spectra for FPI sensors with two stretching lengths of 12 mm (a) and 6 mm (b) and resonant wavelength shifts (c) as a function of strain.

TABLE I. Results of the tensile stress of the silica capillary (SC).

Length of SC L (mm)	Stretching length ΔL (μm)	Maximum strain ε	Maximum stress σ (GPa)
8.9	148.5	0.02	1.20
6.9	143.5	0.02	1.50
9.3	153.5	0.02	1.19

value for all reported fiber-optic strain sensors[18] so far, and the sensitivity could be improved further by enlarging the stretching length or decreasing the interference length for the proposed strain sensor. Meanwhile, the advantage of tunable sensitivity for a prepared sensor has also been demonstrated in Fig. 4. The sensitivity of the sensor with 9.3 μm interference length could be tuned from 1932 to 978 pm/$\mu\varepsilon$ by reducing the stretching length from 12 to 6 mm. Therefore, the strain sensitivity for a prepared sensor could be adjusted conveniently according to the requirement of practical applications.

To obtain the maximum tensile stress of the silica capillary in the proposed sensor, three silica capillaries with different lengths are stretched to rupture apart in our experiments, and the maximum strains are shown in Table I. The maximum tensile strain for the silica capillary is about 0.02, which agrees with the reported values.[25] Therefore, the maximum stretching length for the silica capillary with a length of 12 mm is about 0.24 mm.

Similar to the extrinsic FPI sensor in our previous work,[26] the temperature sensitivity of the demonstrated extrinsic FPI strain sensor is usually less than 1 pm/°C, which benefits from the low thermal expansion coefficient (~0.56×10^{-6}/°C) and small cavity length. The corresponding strain error resulting from ambient temperature fluctuation is 5.2×10^{-4}/°C for the sensor with a cavity length of 9.3 μm and a stretching length of 12 mm. Therefore, the temperature cross sensitivity is very low. In addition, compared with other report strain sensors, the cost of the proposed device is very low because the essential raw materials are the economical SMF and silica capillary and the processing equipment is simple glue fixation.

IV. CONCLUSION

In conclusion, we have experimentally demonstrated an ultrasensitive fiber-optic strain sensor by constructing an extrinsic FPI with a large ratio of stretching length to interference length. The strain sensitivity of the proposed device is up to 1932 pm/$\mu\varepsilon$, which is an order of magnitude higher than the maximum value of all reported fiber-optic strain sensors so far. Meanwhile, the sensitivity could be tailored artificially by changing the stretching length of the sensor. In addition, the cost of the proposed device is very low for the economical processing equipment and raw materials. Therefore, the proposed device shows attractive potential for practical applications.

ACKNOWLEDGMENTS

This work was funded by the National Natural Science Foundation of China (NSFC) (Grant Nos. 12174232, 11804208, U21A6006, and 11774209) and Shanxi 1331KS.

AUTHOR DECLARATIONS

Conflict of Interest

The authors have no conflicts of interest to disclose.

Author Contributions

Shiwei Yang: Data curation (equal); Investigation (equal); Methodology (equal); Writing – original draft (equal). **Qiang Zhang**: Conceptualization (equal); Funding acquisition (equal); Investigation (equal); Writing – review & editing (equal). **Xiaobo Li**: Methodology (equal); Software (equal); Validation (equal). **Quansen Wang**: Formal analysis (equal); Methodology (equal); Validation (equal). **Yongmin Li**: Conceptualization (equal); Funding acquisition (equal); Writing – review & editing (equal).

DATA AVAILABILITY

The data that support the findings of this study are available from the corresponding author upon reasonable request.

REFERENCES

[1] N. J. Lindsey, T. C. Dawe, and J. B. Ajo-Franklin, Science **366**, 1103 (2019).
[2] H. Nakstad and J. T. Kringlebotn, Nat. Photonics **2**, 147 (2008).
[3] L. Albero Blanquer, F. Marchini, J. R. Seitz *et al.*, Nat. Commun. **13**, 1153 (2022).
[4] M. Jones, Nat. Photonics **2**, 153 (2008).
[5] I. García, J. Zubia, G. Durana, G. Aldabaldetreku, M. A. Illarramendi, and J. Villatoro, Sensors **15**, 15494 (2015).
[6] M. Ramakrishnan, G. Rajan, Y. Semenova, and G. Farrell, Sensors **16**, 99 (2016).
[7] P. Roriz, L. Carvalho, O. Frazão, J. L. Santos, and J. A. Simões, J. Biomech. **47**, 1251 (2014).
[8] C. Chen, A. Laronche, G. Bouwmans, L. Bigot, Y. Quiquempois, and J. Albert, Opt. Express **16**, 9645 (2008).
[9] Y. Wang, X. Qiao, H. Yang, D. Su, L. Li, and T. Guo, Sensors **14**, 18575 (2014).
[10] F. L. M. Santos and B. Peeters, Rev. Sci. Instrum. **87**, 102506 (2016).
[11] E. Maccioni, U. Giacomelli, D. Carbone, S. Gambino, M. Orazi, R. Peluso, and F. Sorrentino, Rev. Sci. Instrum. **90**, 094501 (2019).
[12] Y. P. Wang, L. Xiao, D. N. Wang, and W. Jin, Opt. Lett. **31**, 3414 (2006).
[13] W. Liu, H. Du, X. Bai *et al.*, Sens. Actuators, A **299**, 111614 (2019).
[14] X. Chen, W. Chen, Y. Liu *et al.*, IEEE Sens. J. **22**, 3196 (2022).
[15] X. Dong, Z. Luo, H. Du, X. Sun, K. Yin, and J. Duan, Opt. Lasers Eng. **116**, 26 (2019).
[16] C. R. Liao, D. N. Wang, and Y. Wang, Opt. Lett. **38**, 757 (2013).
[17] H. Zhang, Z. Wu, P. P. Shum *et al.*, Sci. Rep. **7**, 46633 (2017).
[18] H. F. Martins, J. Bierlich, K. Wondraczek *et al.*, Opt. Lett. **39**, 2763 (2014).
[19] M. S. Ferreira, J. Bierlich, J. Kobelke, K. Schuster, J. L. Santos, and O. Frazão, Opt. Express **20**, 21946 (2012).
[20] P. Zhang, M. Tang, F. Gao, B. Zhu, S. Fu, J. Ouyang, and P. P. Shum, D. Liu, Opt. Express **22**, 19581 (2014).
[21] S. Liu, K. Yang, Y. Wang, J. Qu, C. Liao, J. He, and Z. Li, G. Yin, B. Sun, J. Zhou, G. Wang, J. Tang, J. Zhao, Sci. Rep. **5**, 7624 (2015).
[22] K. Zhou, M. Z. Ai, Z. H. Qian, X. X. Gao, Z. H. Hu, Q. Li, and G. C. Guo, Appl. Phys. Lett. **113**, 181901 (2018).
[23] C. Zhang, S. Fu, M. Tang, and D. Liu, Opt. Express **28**, 3190 (2020).
[24] T. Yang, Z. Ran, X. He, L. Gan, Z. He, J. Zhu, P. He, Z. Li, and D. Sun, Photonic Sens. **12**, 220418 (2022).
[25] Z. Ma, Z. Wang, H. Liu, F. Pang, Z. Chen, and T. Wang, Opt. Fiber Technol. **52**, 101966 (2019).
[26] Q. Zhang, T. Zhu, Y. Hou, and K. S. Chiang, J. Opt. Soc. Am. B **30**, 1211 (2013).